

Article

Lithium Polysulfide Catalytic Mechanism of AlN/InN Heterojunction by First-Principles Calculation

Lingfeng Ye ¹, Jin Wang ², Zhiping Lin ^{1,*} , Huafeng Dong ¹ and Fugen Wu ^{2,3}

¹ School of Physics and Optoelectronic Engineering, Guangdong University of Technology, Guangzhou 510006, China; 19874208682@163.com (L.Y.); hfdong@gdut.edu.cn (H.D.)

² School of Materials and Energies, Guangdong University of Technology, Guangzhou 510006, China; wangjin_em@163.com (J.W.); wufg@gdut.edu.cn (F.W.)

³ Guangdong Province Key Laboratory of Intelligent Decision and Cooperative Control, Guangzhou 510006, China

* Correspondence: zhipinglphy@gdut.edu.cn

Abstract: To solve the shuttling effect and transformations of LiPSs in lithium–sulfur batteries, heterostructures have been designed to immobilize LiPSs and boost their reversible conversions. In this paper, we have constructed AlN/InN heterojunctions with AlN with a wide band gap and InN with a narrow band gap. The heterojunctions show metallic properties, which are primarily composed of 2s, 2p N atoms and 5s, 5p In atoms. InN has relatively higher adsorptivity for LiPSs than AlN. Reaction profiles show that on the surface of AlN, there is a lower rate-limiting step than on that of InN, from S₈ to Li₂S₆, and a higher rate-limiting step from Li₂S₄ to Li₂S₂, which is more favorable for InN during the reduction from Li₂S₄ to Li₂S₂. The heterojunction can realize the synergistic reaction of trapping–diffusion–conversion for LiPSs, in which AlN traps large Li₂S₈ and Li₂S₆, the heterojunction causes the diffusion of Li₂S₄, and InN completes the conversion of Li₂S₄ to Li₂S.

Keywords: heterojunction; lithium–sulfur battery; first-principles calculation; synergistic reaction



Citation: Ye, L.; Wang, J.; Lin, Z.; Dong, H.; Wu, F. Lithium Polysulfide Catalytic Mechanism of AlN/InN Heterojunction by First-Principles Calculation. *Catalysts* **2024**, *14*, 323. <https://doi.org/10.3390/catal14050323>

Academic Editor: Igor A. Pašti

Received: 3 April 2024

Revised: 6 May 2024

Accepted: 10 May 2024

Published: 14 May 2024



Copyright: © 2024 by the authors. Licensee MDPI, Basel, Switzerland. This article is an open access article distributed under the terms and conditions of the Creative Commons Attribution (CC BY) license (<https://creativecommons.org/licenses/by/4.0/>).

1. Introduction

Along with high theoretical specific capacity and energy density, lithium–sulfur batteries (Li-S batteries) are considered to be the next generation of high-energy batteries for energy storage equipment and electric vehicles [1]. However, the practical application of Li-S batteries suffers from several bad problems, including poor conductivity of active materials (S₈/Li₂S) and a large volume, which expands upon cycling [2]. The reaction kinetics associated with complex lithium polysulfide (LiPSs) transformations is usually tardy and thus follows serious shuttling effect of LiPSs [3]. Many efforts have been implemented in sulfur positive electrode design, diaphragm modification, electrolyte modification and solid electrolytes [4], such as carbon materials [5], carbon doping [6], transition metal oxide [7], transition metal sulfide [8] and transition metal carbon and nitrides [9]. The design aim has improved the ability to capture sulfur in electrodes, to increase conductivity and to prevent polysulfide dissolution [10]. It has been shown that polar materials can effectively reinforce the immobilization of LiPSs. Heterostructures have been designed to immobilize LiPSs and improve their reversible conversions [11,12]. MoP–MoS₂ [13] or NiCoP/CoP [14] heterojunctions with abundant anchoring sites can accelerate both reduction of LiPSs and oxidation of Li₂S. CoSe/ZnSe heterostructures with a negligible band gap show metallic properties and possess a low sulfur reduction energy, which can accelerate redox reaction kinetics during the charging and discharging process [15]. Calculations have been shown that MoS₂ has a wide band gap semiconductor and Ni₃S₂ has metallic properties in MoS₂–Ni₃S₂ heterojunctions and electrochemical exams have been shown that heterojunction have better conductivity and lower interfacial resistance [16].

Moreover, III-nitride semiconductors have attracted extensive attention in ultraviolet light-emitting diodes and high-frequency, high-power transistors [17,18]. AlN is a wide band gap semiconductor with excellent chemical stability and high thermal conductivity [19]. InN is an end-point compound. The optical adsorption edge of sputter-grown InN films has been shown to possess high electron concentration and low electron mobility [20]. Optical synaptic devices based on GaN/AlN periodic structure have shown strong persistent photoconductivity in ultraviolet detection, which is caused by the strong polarization of GaN/AlN heterojunctions [21]. The band gap of AlN/Al₂O₃ heterojunctions has been reduced significantly, making it about 3.9 eV that is owing to the competition between the elongated Al-N and Al-O bonds across the interface. And the incoherent interface can generate a very strong interfacial ultraviolet light emission [22]. In this paper, we have designed a strong polarization AlN/InN heterojunction and studied its ability in terms of LiPS conversion in Li-S batteries in the following sections. We will discuss the adsorption ability of AlN and InN with regard to LiPSs, as well as LiPS conversion capacity at the heterojunction interface.

2. Calculation Method

Calculations are performed based on the DFT method and are executed by VASP [23]. PAW pseudopotentials have been applied to deal with electron-ion interactions [24]. The exchange-correlation interaction between electrons was treated by GGA with the Perdew-Burke-Ernzerhof (PBE) function [25]. To prevent severe band gap underestimation, the hybrid DFT-HSE06 hybridization generalized function is employed to obtain the band gap [26,27]. The electron wave function is unfolded on the basis of plane waves, and E_{cut} is 500 eV. The convergence threshold of total energy and ionic force are 1×10^{-4} eV/Å.

The surface adsorption of LiPSs are constructed on the $3 \times 3 \times 1$ 2D surface of AlN and InN, on which a vacuum layer of 20 Å has been installed to avoid the interaction between images caused by periodic boundaries. In order to obtain the adsorption energy between AlN, InN, AlN/InN heterojunction and LiPSs, the following equations are used:

$$\Delta E_{\text{ads}} = E(\text{suf/LiPSs}) - E(\text{suf}) - E(\text{LiPSs})$$

where $E(\text{suf})$ is the energy of AlN, InN and the heterojunction without adsorbing LiPSs; $E(\text{LiPSs})$ is the energy of the LiPSs; and $E(\text{suf/LiPSs})$ is the energy of the surface structure with the LiPS adsorbate. The Van der Waals interactions between the surface and the LiPSs can be described by the empirical correction scheme of the DFT-D2 (D stands for dispersion) method in the Grimme scheme [28]. The Gibbs free energy of the sulfur reduction reaction was calculated by following equation:

$$\Delta G = \Delta E_{\text{ad}} + \Delta E_{\text{ZPE}} - T\Delta S$$

where ΔE_{ad} is the change in reaction energy obtained by calculation, ΔE_{ZPE} represents the zero-point energy difference, and ΔS represents the entropy difference. Charge transfers between different atoms are illustrated by applying Bader's charge [29].

3. Results and Discussion

3.1. The Band Gap Structure of AlN, InN and AlN/InN Heterojunctions

AlN and InN belong to the triple group of N compounds within the P_{m63} space group. The structure of SL has smaller lattice parameters, a and c , and a shorter bond length than that of bulk AlN and InN, which comes from the stronger interactions between atoms in a single layer. The energy band structures of AlN and InN are shown in Figure 1. It can be seen from Figure 1a,b that the band gap of bulk AlN is 5.4099 eV and the band gap of bulk InN is 0.8016 eV, which is in agreement with other calculations [30] and is smaller than the experimental value [31]. The bulk structures all have direct band gaps located at the Γ point. The band gap of SL (as shown Figure 1c,d) is different, in which the band gap of AlN narrows (4.6731 eV) and that of InN broadens (1.0674). SL structures have an indirect band

gap, which is in agreement with other research showing that the band gap transition from direct to indirect can occur in the transitional metal dichalcogenides [30]. The bonding states at VBM with lower energy are located at Γ , which is composed of hybridized p_x and p_y orbitals. The anti-bonding states at CBM with higher energy are at M.

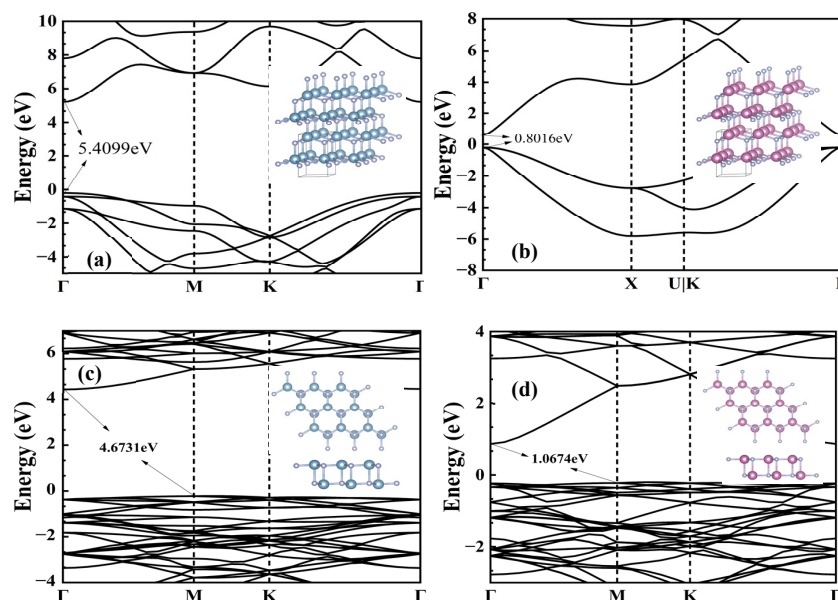


Figure 1. (a,c) are the band structures of the bulk and single-layer AlN; (b,d) are the band structures of bulk and single-layer InN.

The optimization results of constructed monolayer AlN/InN heterojunctions are shown in Figure 2a. The smooth 2D planar configuration of AlN and InN is broken and slightly deformed. Bader charge analysis shows that there are charge transfers before and after the formation of the heterojunction, in which N atoms in the InN obtain more electrons (0.03 e) than 0.01 e for the AlN. The energy band structure of the heterojunction (Figure 2b) shows metallic properties. The calculated density of states has no gap at the Fermi level, as shown in Figure 2c. These states are primarily composed of 2s, 2p N atoms and 5s, 5p In atoms. The contribution of the electronic states of the Al atoms is small. It has been confirmed that the enhancement of the conductivity of a catalyst can promote electron transfer between the components [32].

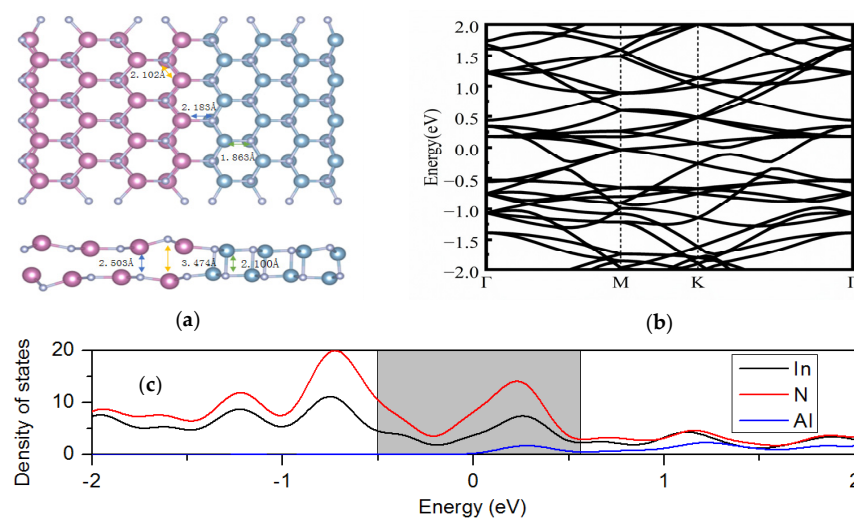


Figure 2. (a) is the structure of AlN/InN heterojunction and its bond length, (b) is the band gap of heterojunction, and (c) is density of states of the In, Al and N atoms.

3.2. Catalytic Mechanism of Li_2S_n for AlN and InN

The optimized structures of five kinds of LiPS adsorbed onto AlN and InN surfaces are obtained; Li_2S , Li_2S_4 and Li_2S_6 are three optimized structures shown in Figure 3. All Li_2S_n ($n = 1, 2, 4, 6, 8$) was optimized, as also shown in Figure 3. It can be seen that the Li atoms of all types of LiPS molecules are directly connected to N atoms, and the S atoms to the metal atoms of Al or In. Along with LiPS adsorption, the surface of the AlN still remains smooth, and for the InN substrates, roughness can be observed on the surface.

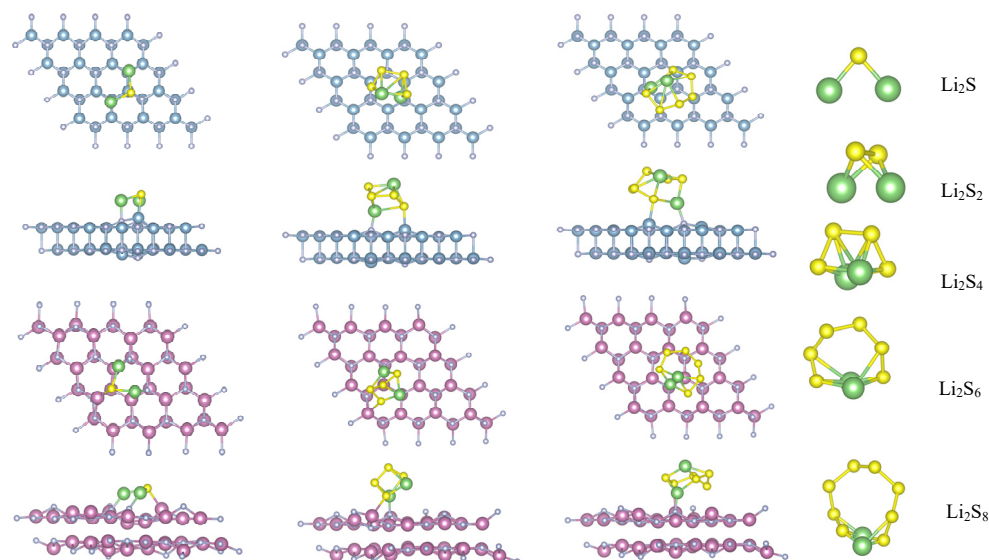


Figure 3. Adsorption structures of LiPSs on AlN and InN for Li_2S_n ($n = 1, 4, 6$) and optimized Li_2S_n molecule structures.

Adsorption energies are calculated to quantitatively evaluate the interaction between Li_2S_n and AlN or InN compounds, as shown in Figure 4. For AlN and InN, the adsorption energies of insoluble $\text{Li}_2\text{S}/\text{Li}_2\text{S}_2$ are lower than those of soluble Li_2S_4 , Li_2S_6 and Li_2S_8 . Along with the stepwise reduction of Li_2S_n , LiPSs+ molecules will accept electrons when adsorbed on the surface of the material. However, AlN has relatively higher adsorptivity for LiPSs than InN does. For the surface of AlN structures, the adsorption energies of Li_2S , Li_2S_2 , Li_2S_4 , Li_2S_6 and Li_2S_8 are -3.02 eV, -2.35 eV, -1.41 eV, -1.35 eV and -1.16 eV, respectively. The adsorption ability of AlN is relatively weaker for all LiPSs molecules, especially for the large molecule Li_2S_n ($n = 4, 6, 8$). The higher adsorption energies of soluble Li_2S_4 , Li_2S_6 and Li_2S_8 mean that the opportunities for transfer electrons from AlN are few and thus retard electrochemical kinetics. Hence, the final product is comparatively difficult to deposit owing to the larger surface energy. In addition, along with the end of the discharge, the number of nuclear sites will be less, and the particle size of the final product, Li_2S , will be large. The adsorption energy is stronger for LiPSs adsorbed on the InN material surface, with values of -8.57 eV, -8.09 eV, -7.61 eV, -6.88 eV and -7.15 eV for Li_2S , Li_2S_2 , Li_2S_4 , Li_2S_6 and Li_2S_8 , respectively. This indicates that adsorption energies are relatively low, and along with the molecular volume becoming larger increase only slightly. This effect of LiPSs volume manifests on the surface of materials, which shows that molecular volume is a contributing factor to adsorption energy. Hence, the chemical interaction between LiPSs and different materials is considered to be the most important of all contributing factors. The lower the adsorption energies of LiPSs are, the better the electrochemical reaction rate is. So, rate performance will be enhanced, and the shuttle effect can be inhibited. The stronger adsorption energy of Li_2S illustrates that its nucleation and precipitation can happen easily on an InN surface. This can be also seen from free energy profiles, as shown in the inset in Figure 4. Reaction profiles from S_8 to Li_2S_6 for AlN have lower rate-limiting steps than InN in the discharge process. And then, the reduction

process from S_8 to Li_2S_6 is thermodynamically more favorable on an AlN surface than on an InN surface. However, there is a rate-limiting step from Li_2S_4 to Li_2S_2 in AlN surface, and it is more favorable for InN during the reduction from Li_2S_4 to Li_2S_2 . Hence, the polarity of semiconducting materials can strengthen the interaction of polar LiPSs with the electrode surface.

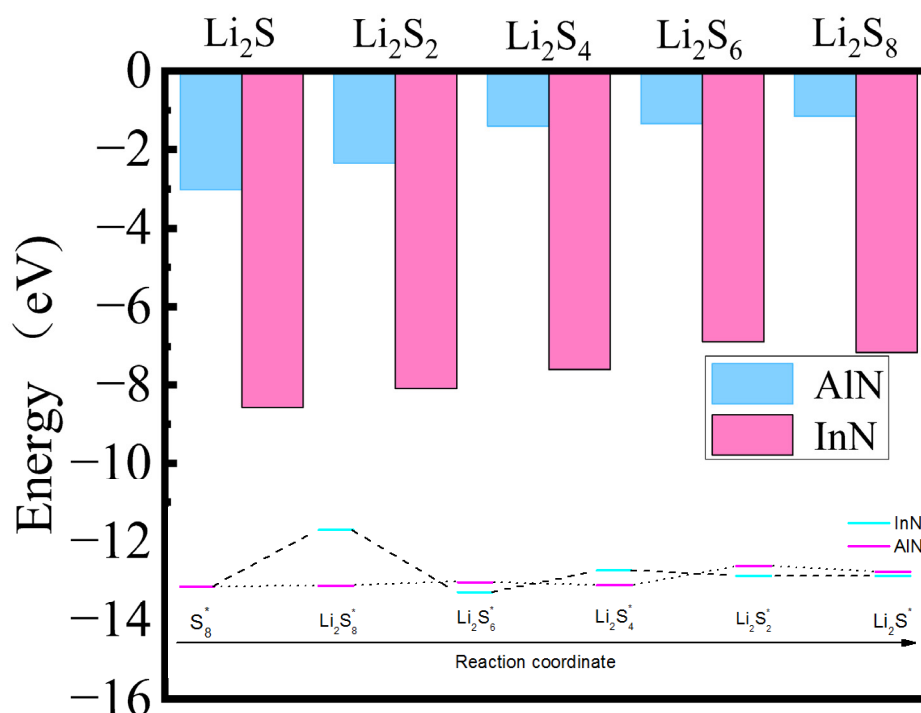


Figure 4. The calculated adsorption energy of Li_2S_n ($n = 1, 2, 4, 6, 8$) on the AlN and InN surface. The inset figure shows energy profiles for the reduction of LiPSs on the AlN and InN surfaces.

To illustrate the interaction between LiPSs and catalytic materials, charge transfers are analyzed using differential charge densities. When LiPSs are adsorbed on the surfaces of materials, the charge densities of the surface around adsorbed Li atoms and S atoms are redistributed, as shown in Figure 5. Li_2S_n , AlN and InN act as electron donors and acceptors, respectively. The electron of AlN and InN will be transferred and the surface structures will be altered during the adsorption process. When LiPS molecules are adsorbed on AlN or InN surfaces, the Li atoms will transfer electrons to their surrounding N atoms and metal atoms. It can be seen from Table 1 that the Al and In will obtain electrons along with Li_2S_n adsorbed on the material surface, and the N atom will lose electrons for small LiPSs (Li_2S and Li_2S_2) and obtain electrons for larger Li_2S_4 , Li_2S_6 and Li_2S_8 . Harvest electrons mean that the unpaired electrons of atoms tend to be saturated, and the electron transition region between S atoms and Al/In atoms during catalysis have the overlapping part of the symmetry-adapted frontier orbitals and a small electron gain region among atoms. For the InN structure, more charges are transferred between Li atoms and N atoms than for the AlN structure, which indicates that the adsorbed Li_2S_n has stronger interactions with the surface of InN. This means that the binding of Li-N is dominated by charge depletion, indicating a strong covalent interaction between Li of LiPSs and N on the surface of materials. Thus, AlN or InN can be used as a good catalytic agent for Li-S batteries, owing to their good adsorption behavior, and can enhance the key reactions of lithium sulfur battery systems.

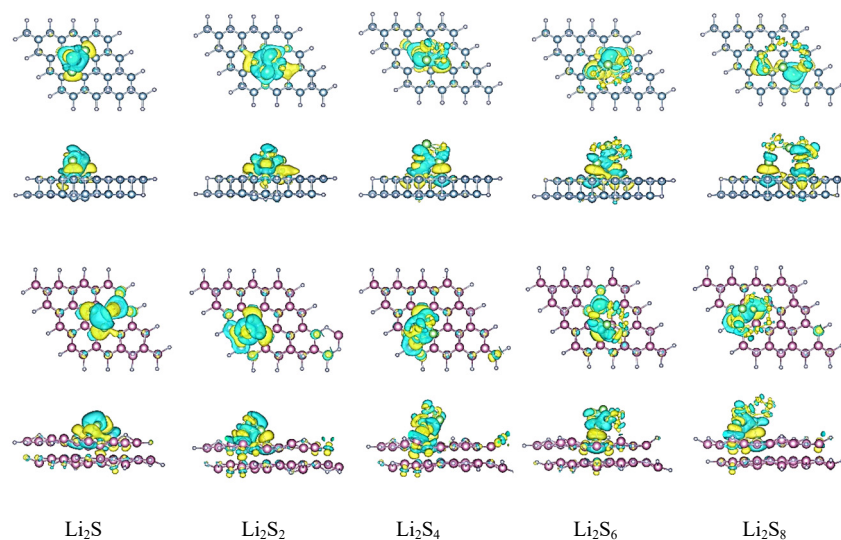


Figure 5. Charge density difference diagram of Li_2S_n ($n = 1, 2, 4, 6, 8$) adsorbed on AlN and InN surfaces.

Table 1. Transfer charges for LiPSs adsorbed on AlN and InN surfaces.

LiPSs	AlN		InN	
	N	Al	N	In
Li_2S	−0.0102 e	0.0291 e	−0.1233 e	0.0474 e
Li_2S_2	−0.0081 e	0.0245 e	−0.1227 e	0.0220 e
Li_2S_4	0.0029 e	0.0077 e	0.1167 e	0.0234 e
Li_2S_6	0.0024 e	0.0188 e	0.1304 e	0.0052 e
Li_2S_8	0.0083 e	0.0071 e	0.1217 e	0.0184 e

3.3. Catalytic Mechanism of Li_2S_n for AlN/InN Heterojunction

Electrocatalysis techniques have been developed to accelerate the sulfur redox reaction. Catalysts, such as metal [33], metal oxides [7], metal sulfides [8], etc., are able to restrict LiPS shuttling and promote sulfur transformation reactions. A heterojunction constructed by dissimilar couplings and different band gaps can meet the above demands for LiPS transformation. It has been reported that heterostructured catalytic cathodes, such as Mn_3O_4 -MnS [34], TiO_2 -TiN [35], have synergistic functions that have been revealed active sites and built-in electric fields in heterogeneous interfaces and form a synergistic effect between the strong adsorption of Mn_3O_4 and the fast conversion of MnS to LiPSs [34]. The twinborn TiO_2 -TiN heterostructure combines the merits of highly adsorptive TiO_2 with conductive TiN and achieves smooth trapping–diffusion–conversion of LiPSs across the interface [35]. Here, heterojunctions constructed with AlN with a broad band gap and InN with a narrow band gap show metallic properties. The adsorbing energy of Li_2S and Li_2S_6 near the junction is calculated, as shown in Figure 6a,b. It can be seen that on the AlN side of the junction, the adsorption energy of the larger Li_2S_6 molecule is lower than that of the small Li_2S molecule, and on the InN side of the junction, the smaller Li_2S molecule has lower adsorption energy, which is agreement with previous research [35]. TiN, with its better conductivity, is favorable for the reversible electrochemical conversion of LiPSs in the charge/discharge process, and TiO_2 , with its relatively poor conductivity, is favorable for the adsorption of LiPSs [35]. This confirms the synergistic effect of AlN and InN. The synergistic process can be illustrated by the reduction process shown in the inset figure of Figure 4. So, AlN traps large Li_2S_8 and Li_2S_6 , the junction causes the diffusion of Li_2S_4 , and InN completes the conversion of Li_2S_4 to Li_2S , which realizes the synergistic reaction of trapping–diffusion–conversion for LiPSs on the surface and interface of the catalytic agent.

Figure 6c shows the three diffusion paths of Li_2S_4 from AlN to InN in the junction, namely PATH1, PATH2 and PATH3. Free energy from adjacent adsorbing sites (Figure 6d) is obtained, which shows the migration abilities of the Li_2S_4 molecule. Larger mobile energy is needed before or after passing through junctions for PATH1 and PATH2. With PATH3, there is lower resistance for migration of Li_2S_4 molecule before or after passing through the junction, and then there is a suitable migration path. As Li_2S_4 molecule is moving across the junction, larger energy is needed to overcome the built-in electric field originating from the interface of the AlN/InN heterojunction, which is favorable for converting polysulfides [36]. It may be to authenticate that the synergistic reaction of trapping–diffusion–conversion for LiPSs has happened, in which AlN traps large Li_2S_8 and Li_2S_6 , the heterojunction causes the diffusion of Li_2S_4 , and InN completes the conversion of Li_2S_4 to Li_2S .

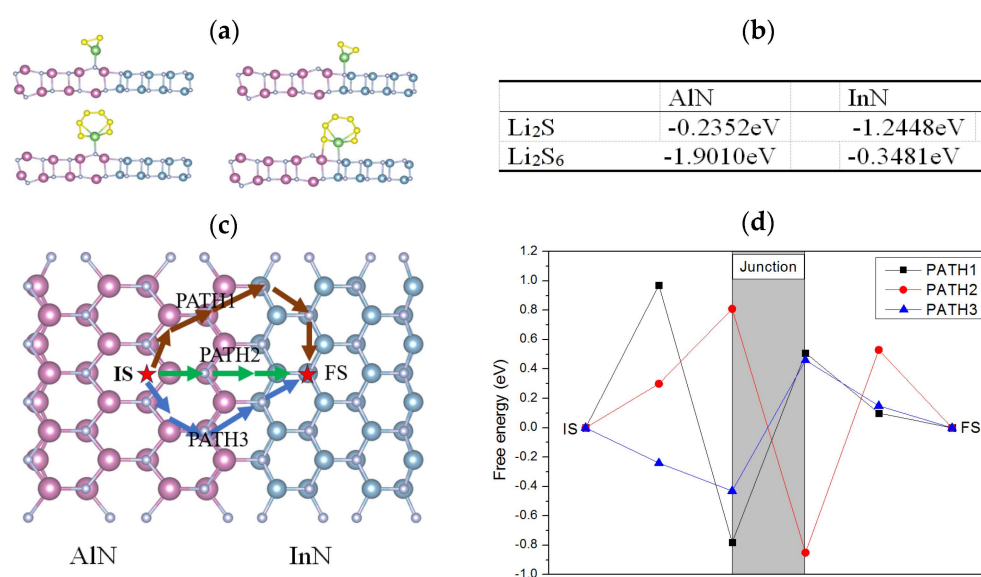


Figure 6. (a) The adsorbing structures of Li_2S and Li_2S_6 in AlN/InN heterojunction, (b) the adsorbing energy of Li_2S and Li_2S_6 near the junction, (c) three diffusion paths of Li_2S_4 from AlN to InN in the junction and (d) the free energy of Li_2S_4 on adjacent adsorption position through different paths, as shown in (c).

4. Conclusions

In summary, the AlN/InN heterojunction constructed by AlN with a wide band gap and InN with a narrow band gap shows better catalytic ability regarding LiPSs in nearby junctions. The energy band structure of the heterojunction shows metallic properties, which are primarily composed of 2s, 2p N atoms and 5s, 5p In atoms and a small contribution of electronic states by Al atoms. AlN has relatively higher adsorptivity for LiPSs than InN. Reaction profiles show that on the surface of AlN S_8 , Li_2S_6 has a lower rate-limiting step than on InN, and Li_2S_4 to Li_2S_2 has a higher rate-limiting step, which is more favorable for InN during the reduction from Li_2S_4 to Li_2S_2 . The adsorbing energy of Li_2S and Li_2S_6 near the junction also illustrates that the AlN side of the junction has stronger adsorption for larger Li_2S_6 molecules, and small Li_2S molecules are favorable for adsorption on the InN side of the junction. The synergistic effect of AlN and InN occurs near the heterojunction, where AlN traps large Li_2S_8 and Li_2S_6 , heterojunction forms diffusion of Li_2S_4 , and InN completes the conversion of Li_2S_4 to Li_2S and realizes the synergistic reaction of trapping–diffusion–conversion for LiPSs on the surface and interface of catalytic agent.

Author Contributions: Conceptualization, Z.L.; Methodology, L.Y. and J.W.; Software, L.Y. and H.D.; Validation, Z.L.; Formal analysis, L.Y., F.W. and Z.L.; Investigation, L.Y. and J.W.; Resources, Z.L. and F.W.; Data curation, L.Y. and Z.L.; Writing—original draft, L.Y.; Writing—review & editing, Z.L. All authors have read and agreed to the published version of the manuscript.

Funding: The Guangdong Province Natural Science Foundation (No. 2018A030313272) through the NSGP Committee of China.

Data Availability Statement: Data are contained within the article.

Acknowledgments: This work was supported by the Network Computing Center of Guangdong University of Technology.

Conflicts of Interest: The authors declare no conflicts of interest.

References

1. Chung, S.H.; Manthiram, A. Current Status and Future Prospects of Metal-Sulfur Batteries. *Adv. Mater.* **2019**, *31*, 1901125. [[CrossRef](#)] [[PubMed](#)]
2. Yan, B.; Li, Y.; Gao, L.; Tao, H.C.; Zhang, L.L.; Zhong, S.K.; Li, X.F.; Yang, X.L. Confining ZnS/SnS₂ Ultrathin Heterostructured Nanosheets in Hollow N-Doped Carbon Nanocubes as Novel Sulfur Host for Advanced Li-S Batteries. *Small* **2022**, *18*, e2107727. [[CrossRef](#)] [[PubMed](#)]
3. Zhang, J.Y.; Xu, G.B.; Zhang, Q.; Li, X.; Yang, Y.; Yang, L.W.; Huang, J.Y.; Zhou, G.M. Mo-O-C Between MoS₂ and Graphene Toward Accelerated Polysulfide Catalytic Conversion for Advanced Lithium-Sulfur Batteries. *Adv. Sci.* **2022**, *9*, e2201579. [[CrossRef](#)]
4. Yang, X.F.; Luo, J.; Sun, X.L. Towards high-performance solid-state Li-S batteries: From fundamental understanding to engineering design. *Chem. Soc. Rev.* **2020**, *49*, 2140–2195. [[CrossRef](#)] [[PubMed](#)]
5. Li, T.T.; He, C.; Zhang, W.X. Rational design of porous carbon allotropes as anchoring materials for lithium sulfur batteries. *J. Energy Chem.* **2021**, *52*, 121–129. [[CrossRef](#)]
6. Hou, T.Z.; Chen, X.; Peng, H.J.; Huang, J.Q.; Li, B.Q.; Zhang, Q.; Li, B. Design Principles for Heteroatom-Doped Nanocarbon to Achieve Strong Anchoring of Polysulfides for Lithium-Sulfur Batteries. *Small* **2016**, *12*, 3283–3291. [[CrossRef](#)] [[PubMed](#)]
7. Tao, X.; Wang, J.; Liu, C.; Wang, H.; Yao, H.; Zheng, G.; Seh, Z.W.; Cai, Q.; Li, W.; Zhou, G. Balancing surface adsorption and diffusion of lithium-polysulfides on nonconductive oxides for lithium-sulfur battery design. *Nat. Commun.* **2016**, *7*, 11203. [[CrossRef](#)]
8. Chen, X.; Peng, H.J.; Zhang, R.; Hou, T.Z.; Huang, J.Q.; Li, B.; Zhang, Q. An Analogous Periodic Law for Strong Anchoring of Polysulfides on Polar Hosts in Lithium Sulfur Batteries: S- or Li-Binding on First-Row Transition-Metal Sulfides? *ACS Energy Lett.* **2017**, *2*, 795–801. [[CrossRef](#)]
9. Wang, D.S.; Li, F.; Lian, R.Q.; Xu, J.; Kan, D.X.; Liu, Y.H.; Chen, G.; Gogotsi, Y.; Wei, Y.J. A General Atomic Surface Modification Strategy for Improving Anchoring and Electrocatalysis Behavior of Ti₃C₂T₂ MXene in Lithium-Sulfur Batteries. *ACS Nano* **2019**, *13*, 11078–11086. [[CrossRef](#)]
10. Wang, Z.K.; Li, Y.; Ji, H.Q.; Zhou, J.Q.; Qian, T.; Yan, C.L. Interwoven MXene nanosheet/carbon-nanotube composites as Li-S cathode hosts. *Adv. Mater.* **2022**, *34*, 2203699. [[CrossRef](#)]
11. Zhang, M.; Chen, W.; Xue, L.X.; Jiao, Y.; Lei, T.Y.; Chu, J.W.; Huang, J.W.; Gong, C.H.; Yan, C.Y.; Yan, Y.C.; et al. Adsorption-Catalysis Design in the Lithium-Sulfur Battery. *Adv. Energy Mater.* **2019**, *10*, 1903008. [[CrossRef](#)]
12. Ng, S.F.; Lau, M.Y.L.; Ong, W.J. Lithium-Sulfur Battery Cathode Design: Tailoring Metal-Based Nanostructures for Robust Polysulfide Adsorption and Catalytic Conversion. *Adv. Mater.* **2021**, *33*, e2008654. [[CrossRef](#)] [[PubMed](#)]
13. Wang, X.X.; Deng, N.P.; Ju, J.G.; Wang, G.; Wei, L.Y.; Gao, H.J.; Cheng, B.W.; Kang, W.M. Flower-like heterostructured MoP-MoS₂ hierarchical nanoreactor enabling effective anchoring for LiPS and enhanced kinetics for high performance Li-S batteries. *J. Membr. Sci.* **2022**, *642*, 120003. [[CrossRef](#)]
14. Li, R.R.; He, J.; Lei, M.; Yang, M.H.; Li, C.L. High-density catalytic heterostructures strung by buried-in carbon tube network as monolithic holey host for durable Li-S batteries. *Chem. Eng. J.* **2022**, *446*, 137294. [[CrossRef](#)]
15. Ye, Z.Q.; Jiang, Y.; Yang, T.Y.; Li, L.; Wu, F.; Chen, R.J. Engineering Catalytic CoSe-ZnSe Heterojunctions Anchored on Graphene Aerogels for Bidirectional Sulfur Conversion Reactions. *Adv. Sci.* **2022**, *9*, e2103456. [[CrossRef](#)] [[PubMed](#)]
16. Wang, J.; Gan, T.; Liao, Y.L.; Wu, F.G.; Lin, Z.P.; Ai, G. Synergistic Catalysis of MoS₂-Ni₃S₂ Heterojunctions to Accelerate Polysulfide Conversion for High-performance Li-S battery. *J. Alloy Compd.* **2023**, *960*, 170546. [[CrossRef](#)]
17. Nakamura, S.; Mukai, T.; Senoh, M. Candela-class high-brightness InGaN/AlGaIn double-heterostructure blue-light-emitting diodes. *Appl. Phys. Lett.* **1994**, *64*, 1687–1689. [[CrossRef](#)]
18. Mishra, U.K.; Parikh, P.; Wu, Y.F. AlGaIn/GaN HEMTs—an overview of device operation and applications. *Proc. IEEE* **2002**, *90*, 1022–1031. [[CrossRef](#)]
19. Liu, C.; Hu, Z.; Wu, Q.; Wang, X.Z.; Chen, Y.; Sang, H.; Zhu, J.M.; Deng, S.Z.; Xu, N.S. Vapor-solid growth and characterization of aluminum nitride nanocones. *J. Am. Chem. Soc.* **2005**, *127*, 1318–1322. [[CrossRef](#)]
20. Tansley, T.L.; Foley, C.P. Optical band gap of indium nitride. *J. Appl. Phys.* **1986**, *59*, 3241–3244. [[CrossRef](#)]
21. Hua, X.Y.; Zheng, J.Y.; Han, X.; Hao, Z.B.; Luo, Y.; Sun, C.Z.; Han, Y.J.; Xiong, B.; Wang, J.; Li, H.T.; et al. Artificial optoelectronic synapse with nanolayered Ga/N/AlN periodic structure for neuromorphic computing. *ACS Appl. Nano Mater.* **2023**, *6*, 8461–8467. [[CrossRef](#)]

22. Yan, X.X.; Jiang, Y.X.; Jin, Q.Q.; Yao, T.T.; Wang, W.Z.; Tao, A.; Gao, C.Y.; Li, X.; Chen, C.L.; Ye, H.Q.; et al. Interfacial interaction and intense interfacial ultraviolet light emission at an incoherent interface. *Nat. Commun.* **2023**, *14*, 2788. [[CrossRef](#)]
23. Kresse, G.; Hafner, J. Ab initio molecular dynamics for liquid metals. *Phys. Rev. B* **1993**, *47*, 558–561. [[CrossRef](#)] [[PubMed](#)]
24. Kresse, G.; Furthmüller, J. Efficiency of ab-initio total energy calculations for metals and semiconductors using a plane-wave basis set. *Comput. Mater. Sci.* **1996**, *6*, 15–50. [[CrossRef](#)]
25. Perdew, J.P.; Burke, K.; Ernzerhof, M. Generalized gradient approximation made simple. *Phys. Rev. Lett.* **1996**, *77*, 3865–3868. [[CrossRef](#)] [[PubMed](#)]
26. Batista, E.R.; Heyd, J.; Hennig, R.G.; Uberuaga, B.P.; Martin, R.L.; Scuseria, G.E.; Umrigar, C.J.; Wilkins, J.W. Comparison of screened hybrid density functional theory to diffusion Monte Carlo in calculations of total energies of silicon phases and defects. *Phys. Rev. B* **2006**, *74*, 121102. [[CrossRef](#)]
27. Heyd, J.; Scuseria, G.E. Efficient hybrid density functional calculations in solids: Assessment of the Heyd–Scuseria–Ernzerhof screened Coulomb hybrid functional. *J. Chem. Phys.* **2004**, *121*, 1187–1192. [[CrossRef](#)]
28. Grimme, S. Semiempirical GGA-type density functional constructed with a long-range dispersion correction. *J. Comput. Chem.* **2006**, *27*, 1787–1799. [[CrossRef](#)]
29. Sanville, E.; Kenny, S.D.; Smith, R.; Henkelman, G. Improved grid-based algorithm for Bader charge allocation. *J. Comput. Chem.* **2007**, *28*, 899–908. [[CrossRef](#)]
30. Bacaksiz, C.; Sahin, H.; Ozaydin, H.D.; Horzum, S.; Senger, R.T.; Peeters, F.M. Hexagonal AlN: Dimensional-crossover-driven band-gap transition. *Phys. Rev. B* **2015**, *91*, 085430. [[CrossRef](#)]
31. Vurgaftman, I.; Meyer, J.R. Band parameters for nitrogen-containing semiconductors. *J. Appl. Phys.* **2003**, *94*, 3675–3696. [[CrossRef](#)]
32. Zhang, D.; Wang, S.; Hu, R.M.; Gu, J.A.; Cui, Y.L.S.; Li, B.; Chen, W.H.; Liu, C.T.; Shang, J.X.; Yang, S.B. Catalytic conversion of polysulfides on single atom zinc implanted MXene toward high-rate Lithium-sulfur batteries. *Adv. Funct. Mater.* **2020**, *30*, 2002471. [[CrossRef](#)]
33. Du, Z.Z.; Chen, X.J.; Hu, W.; Chuang, C.H.; Xie, S.; Hu, A.J.; Yan, W.S.; Kong, X.H.; Wu, X.J.; Ji, H.X.; et al. Cobalt in nitrogen-doped graphene as single-atom catalyst for high-sulfur content lithium-sulfur batteries. *J. Am. Chem. Soc.* **2019**, *141*, 3977–3985. [[CrossRef](#)]
34. Qin, B.; Wang, Q.; Yao, W.Q.; Cai, Y.F.; Chen, Y.H.; Wang, P.C.; Zou, Y.C.; Zheng, X.H.; Cao, J.; Qi, J.L.; et al. Heterostructured Mn₃O₄-MnS multi-shelled hollow spheres for enhanced polysulfide regulation in lithium-sulfur batteries. *Energy Environ. Mater.* **2023**, *6*, e12475. [[CrossRef](#)]
35. Zhou, T.H.; Lv, W.; Li, J.; Zhou, G.M.; Zhao, Y.; Fan, S.X.; Liu, B.L.; Li, B.H.; Kang, F.Y.; Yang, Q.H. Twinborn TiO₂-TiN heterostructures enabling smooth trapping-diffusion-conversion of polysulfides towards ultralong life lithium-sulfur batteries. *Energy Environ. Sci.* **2017**, *10*, 1694–1703. [[CrossRef](#)]
36. Xiong, W.M.; Lin, J.D.; Wang, H.Q.; Li, S.; Wang, J.H.; Mao, Y.X.; Zhan, X.; Wu, D.Y.; Zhang, L. Construction of strong built-in electric field in binary metal sulfide heterojunction to propel high-loading lithium-sulfur batteries. *J. Energy Chem.* **2023**, *81*, 492–501. [[CrossRef](#)]

Disclaimer/Publisher’s Note: The statements, opinions and data contained in all publications are solely those of the individual author(s) and contributor(s) and not of MDPI and/or the editor(s). MDPI and/or the editor(s) disclaim responsibility for any injury to people or property resulting from any ideas, methods, instructions or products referred to in the content.